Electronic and adsorption properties of extended chevron and cove-edged graphene nanoribbons

H. Abdelsalam[1,2], V. A. Saroka[3,4], N. H. Teleb[5],M. Ali[6], W. O. Younis[7], Q. Zhang[1*]

[1]School of Materials Science and Engineering, Yancheng Institute of Technology, Yancheng 224051, P. R. China. E-mail: qfangzhang@gmail.com

[2]Theoretical Physics Department, National Research Centre, El-Buhouth Str., Dokki,Giza, 12622, Egypt

[3]Institute for Nuclear Problems, Belarusian State University, Bobruiskaya 11, 220030 Minsk, Belarus

[4]Center for Quantum Spintronics, Department of Physics, Norwegian University of Science and Technology, NO-7491 Trondheim, Norway

[5]Electron Microscope and Thin Films Department, National Research Centre, El-Buhouth Str., Dokki, Giza, 12622, Egypt.

[6]Basic Sciences Department, Misr University for Science and Technology, Giza, 77, Egypt.

[7]Vice Presidency for Postgraduate Studies and Scientific Research, Imam Abdulrahman Bin Faisal University, P.O. Box 1982, Dammam, 31441, Saudi Arabia.

Abstract

The electronic and adsorption properties of chevron and cove-edged graphene nanoribbons (GNRs) are studied using first principles calculations. The positive binding and adsorption energies in conjunction with the positive infrared frequencies insure the stability of the considered GNRs. The results show that the binding strength of coved-edged GNRs is higher than that of chevron ones because the morphology of the latter requires a higher number of C-atoms at the edges than the former. The edge atoms in chevron GNRs create interactive edge states that significantly decreases the energy gap (Eg=0.03 eV) with respect to the wide gap between bulk states in cove-edged ones (Eg=2.19 eV). The molecular orbitals distributions of these edge states are localized only on the arms of the nanoribbon making it a potential topological insulator. The energy gap between bulk states in cove-edged decreases by increasing the width due to quantum size effect, while in chevron GNRs the gap between edge states increases because of the interaction among these states. The adsorption of methylene blue shows interesting properties depending on the type of the nanoribbons, the interaction position, and the attached chemical group. The interactive edge states provide moderate adsorption on the arms of the nanoribbons and the attached chemical groups enhance the adsorption by adding new adsorption positions. The additional molecular orbitals from the physically adsorbed dye lower the band gap and create semimetal GNRs with zero or negative band gap.

Keywords: Extended chevron and cove-edged; Graphene nanoribbons; DFT; electronic and adsorption properties; methylene blue adsorption.

1. Introduction

Graphene nanoribbons (GNRs) are quasi-one-dimensional structures of graphene that can be now produced with the atomic precision in a great variety of forms and geometries [1]. The most successful methods realize bottom-up synthesis on metallic substrate [2] or in solution [3,4]. The two simplest geometries of GNRs with straight *zigzag* [5] and *armchair* [2,6,7] edges have been obtained with atomic precision. Recently, several representatives of monolayer GNRs of zigzag-shape class [8–11] have also been produced: Z60 [12], Z120 [13], A60 [14,15], A120 [16,17].

Graphene nanoribbons are famous for their spin-polarized **edge states** at the *zigzag* edges [18,19]. These states are ideal for applications in spintronics [20] and quantum computing [21]. The p_z-nature of edge states and high fraction of zero spin nuclei in host materials with up to 99 % of ^{12}C lead to a negligible hyperfine interaction eliminating the major source of decoherence [22]. It was recently demonstrated that such edge states in functionalized atomically precise GNRs can be coherently manipulated and they preserve coherence up to milliseconds at room temperature [23].

The edge states may be intimately related to topology. In this case, the existence of the edge modes crossing the band gap in systems with edges is usually predicted by a topological invariant that is calculated on the bulk states of the periodic system without edges. This is so-called bulk-boundary correspondence principle [24–26]. The topological edge states characterized by Chern invariant plays key role in integer quantum Hall effect [27,28]. Similar Hall conductance quantization can be achieved with a zero average magnetic field in Haldane model [29]. It has been shown that the graphene Hamiltonian accounting for the spin-orbit interaction reduces for each spin to Haldane model. When spin-orbit interaction is included, the spin-filtered edge states localized at the graphene zigzag edges becomes topological. As a result the quantum spin Hall effect [30,31] and the quantum spin Hall phase can be distinguished from normal insulating phase by the topological Z_2 invariant [32]. Zero chiral modes localized at the *zigzag* edges can also form under the locally applied external electrostatic field and can be easily manipulated with the field [33]. These modes are also of topological nature but they are characterized by different topological invariant called valley-dependent topological charge [34] The topological charge is different from Chern number or Z_2 invariant. The edge states due locally applied potential have been also reported for GNRs with *zigzag*, *armchair* and *bearded* edges [35]. These states can coexist with topological edge states due to the spin-orbit interaction. The primary technological interest in topological edge states is that due to the absence of the back scattering they form ideal channels of ballistic conductance. Such channels are not sensitive to impurities and disorder.

The topological description of the edge states is not always robust. The clear difference between the bulk and edge states vanishes in non-Hermitian systems due to the non-Hermitian skin effect [36,37] and new topological invariants are needed to characterize such systems. Similarly, there is a problem with non-periodic structures [38]. The edge states are widely spread in quantum dots. Such states have been reported in many 2D material based quantum dots: graphene [39–43], silicene [43–45] and phosphorene [46–51]. However, due to the lack of periodicity and absence of the Brillouin zone, the definitions of the standard topological invariants are not applicable. Therefore, there is an ongoing effort to find an invariant defined in the real space that can be applied to non-periodic and disordered systems [38,52].

Boundaries between distinct topological phases can host localized states that are very much like edge states. Such boundaries can form at the interfaces between the two ribbons or between the ribbon and the vacuum. In the latter case, the localized mode should appear at the ends of finite length ribbon. The topological phases of 1D GNRs with straight edges have been theoretically classified with Z_2 topological invariant [53]. It has been shown experimentally that interfaces between different width armchair GNRs hosing in-gap localized states can be used for engineering of one-dimensional bands in superlattices of GNR junctions [54]. Similar topological band construction relying on Z_2 topological invariant has been demonstrated for a one-dimensional Su-Schrieffer-Heeger model realized at the edges of the armchair GNRs [55]. On the other hand, the in-gap edge states without clear topological origin have been detected at the *zigzag* ends of finite length armchair GNRs [56].

The topological phases have been recently investigated for zigzag-shaped ribbons Z60 (cove-edge) and A60 (extended chevron), and their junctions with straight *zigzag* and *armchair* GNRs [57]. As in previous work [53], the topological properties are characterized there by Z_2 invariant. However, as follows from the literature review above, the Z_2 topological invariant is not the only possible invariant and, in principle, it does not allow one to predict the edge states with absolute certainty. The edge states may exist but not be topological. From chemistry point of view, even non-topological edge states can be of great practical use. For instance, they can increase the molecule reactivity and facilitate sensor applications. In particular, the localized edge states related to highest occupied molecular orbital (HOMO) or lowest unoccupied molecular orbital (LUMO) determine the most probable areas of electrophilic and nuleophilic substitutions [58]. Recently, it has been shown that A60 ribbons demonstrate enhanced sensing of low molecular weight alcohols (methanol, ethanol) [14]. Such sensors possess impressive 1200% electrical response presumably due to the enhanced edge adsorption of the molecules and the longer edge due to their peculiar form. In the numerical analysis of Ref. [14], however, the A60 GNRs are treated as infinitely long and periodic even though the distance between the electrodes of the sensor is larger than the length of A60 GNRs. In this case, the question of finite-length effects arises, because, for instance, our theoretical calculations for Z120 and A120 GNRs infer that the edge states should exists at the ends of finite length zigzag-shaped GNRs Z120 [59].

It is the purpose of this paper to investigate in detail the electronic properties of A60 zigzag-shaped GNRs using first principles calculations in search of peculiar edge states and enhanced adsorption properties. In what follows, we show that despite being topologically trivial as characterized by Z_2 invariant [57], the ends of the A60 supports robust edge states. Also, the energy gap between the edge states in A60/Z60 GNRs increases/decreases with the GNR width. The selected GNRs show strong capability to adsorb methylene blue dye on the edges and surfaces with high adsorption energy and negligible deformation making them potential applicants in the field of wastewater treatment.

2. Computational model

The present work uses density functional theory [60, 61] as implemented in Gaussian 16 [62] to discuss the physical properties of chevron and cove-edged GNRs. The B3LYP [63,64] is employed in our study as a well-tested hybrid functional that shows a good representation of the electronic properties of C-based and similar 2D materials [65,66]. It is reported that the 3-21g basis set is adequate in size for c-based 2D-materials when considering both computational power and

accuracy [67,68]. For example, the energy gap of the simplest GNR considered here, A60-4-L4, equals 0.0786 eV using the 3-21g basis set and equals 0.0784 eV using the 6-31g basis set. While the computational time is one-quarter higher in the latter that increases even more in larger systems or after interactions with MB, therefore we utilize 3-21g basis set in the calculations.

3. Results and discussion

We investigate the stability, electronic, and adsorption properties of finite chevron (A60) and cove-edged (Z60, Z60R) GNRs. A graphical representation of the GNRs are shown in Fig. 1. Instead of writing the full definition of GNRs, such as A60(3,3,3)L3, Z60(3,3,2.)L3, Z60R(4,4,2)L3, we simply express them as A60-3-L3, Z60-2-L3, and Z60R-2-L3 where the first part represents the GNRs type (chevron/cove-edged), the second is the width, and the third is the length. The electronic properties are investigated by considering the density of states (DOS) and molecular orbitals distributions. In DOS plots, each electronic molecular orbital($\in_i$)is represented by a Gaussian wave function$\frac{1}{\sqrt{2\pi\alpha}}\exp\left[-\frac{(\in-\in_i)^2}{2\alpha^2}\right]$, the broadening $\alpha = 0.032\ eV$. The fermi level is set to zero, $E_F = (E_{HOMO}+E_{LUMO})/2$. The application of GNRs in the field of wastewater treatment are investigated by considering their capability to adsorb large polluting molecules such as methylene blue (MB) dye.

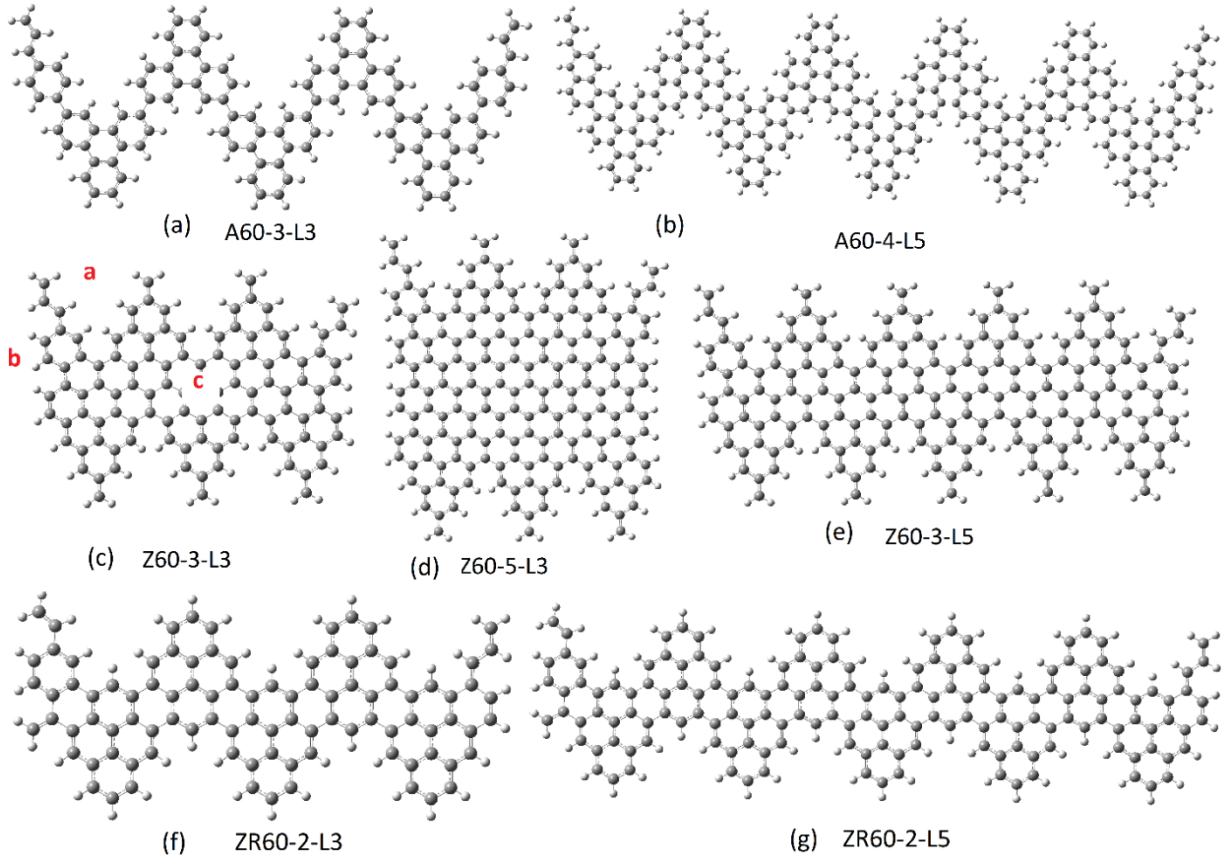

Fig. 1. Optimized structures of extended chevron (A60) and cove-edged (Z60 and Z60R) GNRs with different widths and lengths.

3.1. Stability and Electronic Properties

The binding energy (E_b) for the optimized chevron and coved-edge GNRs in Table 1 is calculated and used to insure the stability of the selected structures. Moreover, it can be used to study the effect of different factors that enhance/ lower the binding strength. The positive binding energy (see Table 1) implies a stable structure. In addition to $E_{b,,}$ the infrared spectra for some GNRs (Fig. 4 in Appendix A), with positive frequencies indicate that the structures are geometrically stable without saddle points on the potential energy surface. The binding energy are calculated from, $E_b = (N_H E_H + N_C E_C - E_G)/N$ where N_H, N_C, N is the number of hydrogen, carbon, and total number of atoms in the GNRs, respectively. E_H, E_C, and E_G are the corresponding energies. The values of E_b in Table 1 indicate that the binding strength of Z60R >Z60>A60. The morphology of A60 requires a higher number of C-atoms at the edges than that in cove-edged GNRs. C atoms at the edges form only two sigma bonds with adjacent C-atoms while at the interior they form three bonds, therefore GNRs with higher number of edge atoms will have lower binding energy. On the other hand, a higher number of edge C-atoms is useful for sensors and wastewater applications due to the higher number of interactive electrons at the edges that enhance the adsorption of gases or pollutants.

Table 1. Binding energy (E_b) and energy gap (E_g) of A60, Z60, and Z60R nanoribbons with various widths and lengths.

Structure (A60)	**E_b(eV)**	**E_g(eV)**	**Structure (Z60)**	**E_b(eV)**	**E_g(eV)**	**Structure (Z60R)**	**E_b(eV)**	**E_g(eV)**
A60-3-L3	6.53	0.08	Z60-2-L3	6.51	1.56	Z60R-2-L3	6.96	2.24
A60-4-L3	6.91	0.08	Z60-3-L3	6.97	0.69	Z60R-3-L3	7.38	1.36
A60-5-L3	7.18	0.19	Z60-4-L3	7.25	0.31	Z60R-4-L3	7.63	0.86
A60-6-L3	7.39	0.25	Z60-5-L3	7.45	0.20	Z60R-5-L3	7.79	0.56
A60-4-L4	6.96	0.06	Z60-3-L4	5.23	0.68	Z60R-2-L4	7.02	2.21
A60-4-L5	6.99	0.05	Z60-3-L5	7.09	0.66	Z60R-2-L5	7.06	2.20
A60-4-L6	7.01	0.04	Z60-3-L6	7.12	0.65	Z60R-2-L6	7.09	2.19
A60-4-L7	7.02	0.03	Z60-3-L7	7.14	0.64	Z60R-2-L7	7.11	2.19

These interactive edges states appear in the highest occupied molecular orbital (HOMO) in Fig. 2 (d) as localized cubs at the arms of the GNRs. These edge states are localized around fermi energy (see Fig. 2 b) and result in a very small energy gap Eg~0.08 eV in A60-3-L3. This tiny energy gap continues decreasing with length increase, reaching 0.03 eV for A60-4-L7. Therefore, these nanoribbons are promising applicants for topological insulator because they are perfect conductor at the arms and insulator at the interior. Although increasing the nanoribbon width leads to increase of the band gap between the edge states, Eg=0.25 in A60-3-L3, however this enlarged gap does not affect the nature of the states as seen from HOMO distribution in Fig. 2 e.

These edge states totally disappear in Z60 and Z60R leading to the formation of wide band gaps (Fig. 2 c, h) between the extended buck states that distribute on the edges and the interior of the GNRs as seen by the HOMO distributions in Fig. 2 (f, k). In deep contrast to the edge states, the band gap between these bulk states decreases by increasing width. Normally, this decrease should be the right behavior of the band gap as a result of the quantum size effect. The gap between the bulk states even in A60 also decreases from ~4 eV (Fig. 2 a) to 2.3 eV (Fig. 2 b). Therefore, the peculiar effect of energy gap increasing with width increasing is related only to edge states that may arise from the interaction among the states themselves. By increasing the width in Z60 and Z60R GNRs the edge states start to appear due to the formation of zigzag edges on which the localized edge states distribute as seen in Fig. 2 (k).

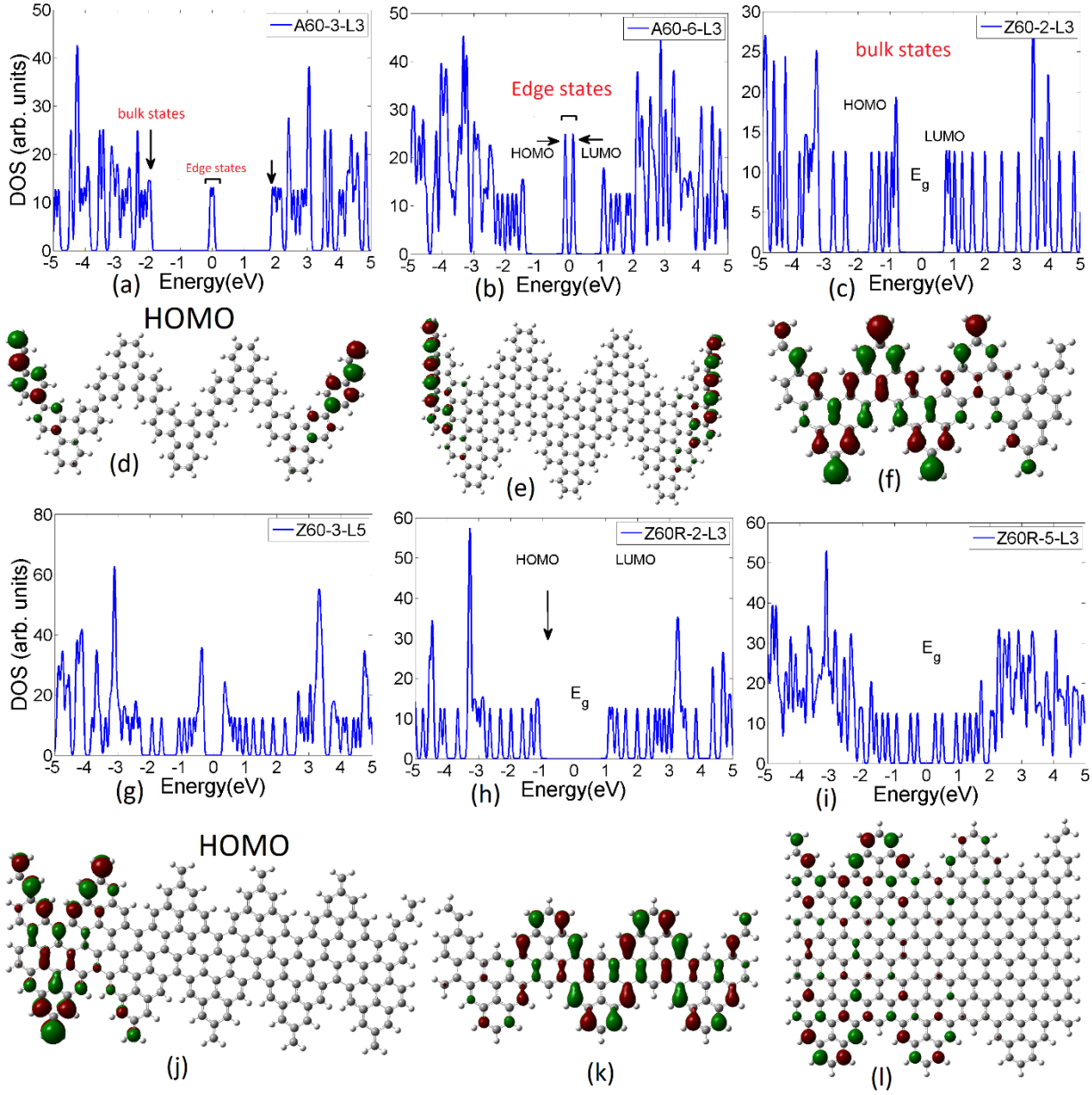

Fig. 2. Electronic density of states and highest occupied molecular orbital of selected GNRs to show the edge/bulk states and the variations in the energy gap.

3.2 Adsorption Properties

The interaction between the GNRs and methylene blue (MB) is investigated to highlight the adsorption competence of GNRs toward such large molecules and the effect of this interaction on the electronic properties. The dispersion interaction is considered through adding Grimmes's dispersion correction (gd3) to the B3LYP-functional [69]. Various adsorption techniques are considered; adsorption of MB through different positions (see Fig. 1 (c) for three adsorption positions, front (a), side (b), and surface (c)) and adsorption after attaching chemical groups (COOH, CN, NO) to the edges. Fig. 3 shows the optimized structures of some GNRs adsorbing MB from different positions (Fig. 3 a-c) and after attachment of COOH and NO groups (Fig. 3 d-f). Table 2 presents the calculated parameters for all the considered interactions between MB and GNRs, namely the adsorption energy (E_a), the Hirshfield [70] charge transfer from the positively charged MB to the GNRs (ΔQ= MB charge before adsorption-MB charge after adsorption) and the energy gap (E_g).

Table 2. The adsorption energy (Ea), the Hirshfield charge transfer (ΔQ), and energy gap (E_g) of A60, Z60, Z60 GNRs adsorbing MB.

Structure + MB		**E_a (eV)**	**ΔQ (e)**	**E_g(eV)**
A60-4-L3- a	-MB	0.0413	0.4351	0.0871
A60-4-L3- b		0.0398	0.5663	0.0816
A60-4-L3- c		0.0413	0.2654	-0.3891
A60-4-L3- a-COOH		0.0381	0.3127	0.0798
A60-4-L3- b-COOH		0.0383	0.2423	0.077
A60-4-L3- a-CN		0.0414	0.3003	0.0797
A60-4-L3- a-NO		0.0360	0.4638	-1.6909
Z60-4-L3 –a		0.0635	0.3792	0.2095
Z60-4-L3 -b		0.0653	0.3061	0.2261
Z60-4-L3 -c		0.0650	0.3054	0.2422
Z60-4-L3-a-COOH		0.0442	0.1953	0.2041
Z60-4-L3 –a-CN		0.0601	0.1830	0.2177
Z60-4-L3 –a-NO		0.0450	0.2852	0.2122
Z60R-3-L3 -a		0.0470	0.3043	0.6346
Z60R-3-L3 -b		0.0452	0.2277	0.3755
Z60R-3-L3 -c		0.0472	0.3322	1.0286
Z60R-3-L3-a-COOH		0.0408	0.0774	-0.3129
Z60R-3-L3 –a-CN		0.0444	0.2200	0.1905
Z60R-3-L3 –a-NO		0.0401	0.1778	0.0082

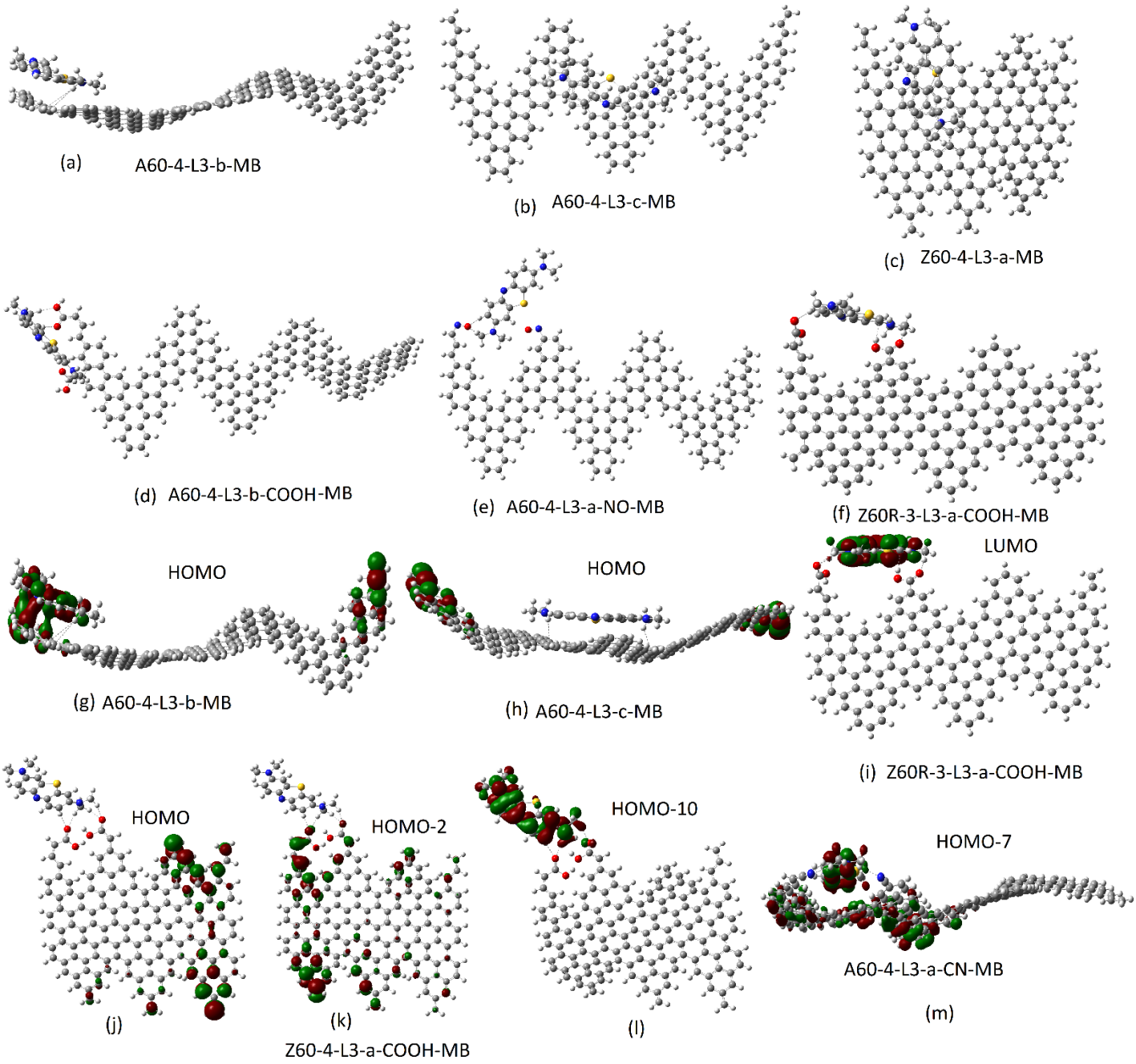

Fig. 3. Optimized structures of chevron and cove-edged GNRs adsorbing methylene blue on different positions and on attached chemical groups (a-f). The molecular orbitals in (g-m) are mainly to present the orbitals resulting from the interaction between the nanoribbons and MB and their position in the valance band with respect to the HOMO.

The adsorption energy per atom is obtained from, $Ea= (E_{GNRs}+E_{MB} -E_{GNRs-MB})/ N$ where E_{GNRs}, $E_{MB,}$ and $E_{GNRs-MB}$ are the total energies of GNRs before adsorption, MB, and GNRs after adsorption, respectively. The positive values of Ea in addition to the positive frequencies from IR spectra shown in Fig. 4 in Appendix A insure a successful adsorption process. Moreover, the

adsorption strength depends on the adsorption position and the type of attachment. The adsorption energy in A60-4-L3- a/-b positions is lower than in A60-4-L3- c while charge transfer in the former is significantly higher. The reason is that in edge adsorption, MB is adsorbed by lower number of C-atoms compared to surface adsorption (see Fig. 3 a, b) which increases E_a in the latter case. ΔQ does not follow that rule because of the different type of interacting energy states. Where in the former case the states are highly interactive edge states that mix with that from MB, see the HOMO distribution in Fig. 3 (g), while the extended surface states provide lower mixing with MB and the HOMO cubes distribute only on the GNRs as in Fig. 3 (h). Therefore, the interactive edge states at the arms of A60 make GNRs potential applicant for applications requiring moderate adsorption such as oxygen evolution reaction. It is observed from Fig. 3 (a) that the adsorption of MB through positions-b (also in position-a) ended up on the left arm of the nanoribbons implying that the adsorption of large molecules requires interaction with additional C-atoms at the surface. The same happened with Z60 and Z60R, see Fig. 3 c. Adsorption of MB at positions-a and-b without any support from surface atoms can be achieved by attaching chemical groups such as COOH and NO in Fig 3. (d, e). Therefore, functional groups enhance the adsorption process by adding new adsorption positions. The adsorption energy and charge transfer in these new adsorptions are slightly lower than other cases, as in Table 2, due to the fewer number of edge atoms involved in the interaction.

The distribution of the HOMO in all the adsorption cases is on the edges, this indicate that even the physically adsorbed MB form more stable molecular orbitals (that distribute on MB) with lower energies than that formed by the edge states. For example, the formed molecular orbitals on the adsorbed MB in Z60-4-L3-a-COOH-MB and A60-4-L3-a-CN are HOMO-10 and HOMO-7, respectively, which are deeper in the valance band than HOMO from the edge states as shown in Fig. 3 (j-m). Only when MB is adsorbed at the arms of A60 (Fig. 3 g) the HOMO distributed on both the GNR and MB due to the direct interaction between the edge states and MB.

The energy gap of GNRs decreases after the adsorption due to the addition of molecular orbitals from the physically adsorbed dye, these orbitals reside inside or around the energy gap and decrease it. The new E_g depends on the type of the nanoribbon, the adsorption position, and the attached chemical group. It becomes very narrow, Eg=0.008 eV in Z60R-3-L3 –a-NO-MB, or narrow Eg=0.204 in Z60-4-L3 –a-COOH-MB, or moderate Eg=1.027 in Z60R-3-L3 –c. The interaction with MB can even lead to transformation from semiconductor to semimetal with negative energy gaps as in A60-4-L3- c and Z60R-3-L3-a-COOH in Table 2. In these systems the orbitals from the MB appear as the LUMO, Fig. 3 i, which mean that the weakly adsorbed MB adds its molecular orbital in the tiny band gap leading to overlap between some orbitals from valance and conduction bands. It is worth noting that for the very narrow Eg=0.008 eV in Z60R-3-L3 –a-NO-MB, the LUMO is also from MB similar to that in Fig. 3i. Thus the resultant materials could be considered as heterostructures with interactive states that result in a zero or negative band gab [71-73].

4. Conclusion

The electronic and adsorption properties of extended chevron and cove-edged graphene nanoribbons are investigated using density functional theory calculations. The effects of width/length, attaching chemical group, and interaction with large molecules such as MB are taken into account. The stability of the structures is confirmed by the positive binding energy and frequencies in the infrared spectrum. The binding energy of chevron GNRs is lower than that of cove-edged ones because of the higher number of edge C-atoms in the former that form only two sigma bonds with adjacent C-atoms. The characteristic edge atoms in chevron nanoribbons create highly interactive edge states that extremely decreases the band gap (Eg~0.03 eV) with respect to the wide band gap between bulk states in cove-edged nanoribbons (Eg~2.19 eV). The molecular orbitals from these states distributes only on the arms of the GNRs making them potential topological insulators. Interestingly, the energy gap between edge states in chevron GNRs increases by increasing width, which contradict the normal behavior of decreasing the gap due to quantum size effect as in coved-edged nanoribbons. Increasing width enlarges the zigzag edge which in turn increases the number of edge states. Then the peculiar increase in the band gap could be due to the enhanced interaction between the edge states. Methylene blue is successfully adsorbed by GNRs and demonstrates interesting electronic and adsorption properties. For instance, edge states provide moderate adsorption on the arms of the nanoribbons and the attached chemical groups improve the adsorption by providing new adsorption positions. The electronic band gap decrease by the adsorption process because of the additional molecular orbital from the adsorbed MB, these orbitals reside inside or around the energy gap and decrease it. The interaction with MB can even lead to transformation from semiconductor to semimetal with zero or negative energy gap.

Acknowledgement

This work is supported by Postgraduate Education Reform Project of Jiangsu Province. HA acknowledges the postdoctoral funding by Talent Young Scientist Program (TYSP). VAS acknowledges support by the Research Council of Norway Centre of Excellence (project no. 262633, “QuSpin”) W. O. Younis (originally affiliated to Physics Department, Faculty of Science, Beni-Suef University, Beni-Suef City, Egypt) acknowledges the collaborative research between Beni-Suef University and IAU.

Appendix A

Infrared spectra of selected chevron and edge-coved GNRs before and after adsorption of MB with positive adsorption frequencies are shown in Fig. 4.

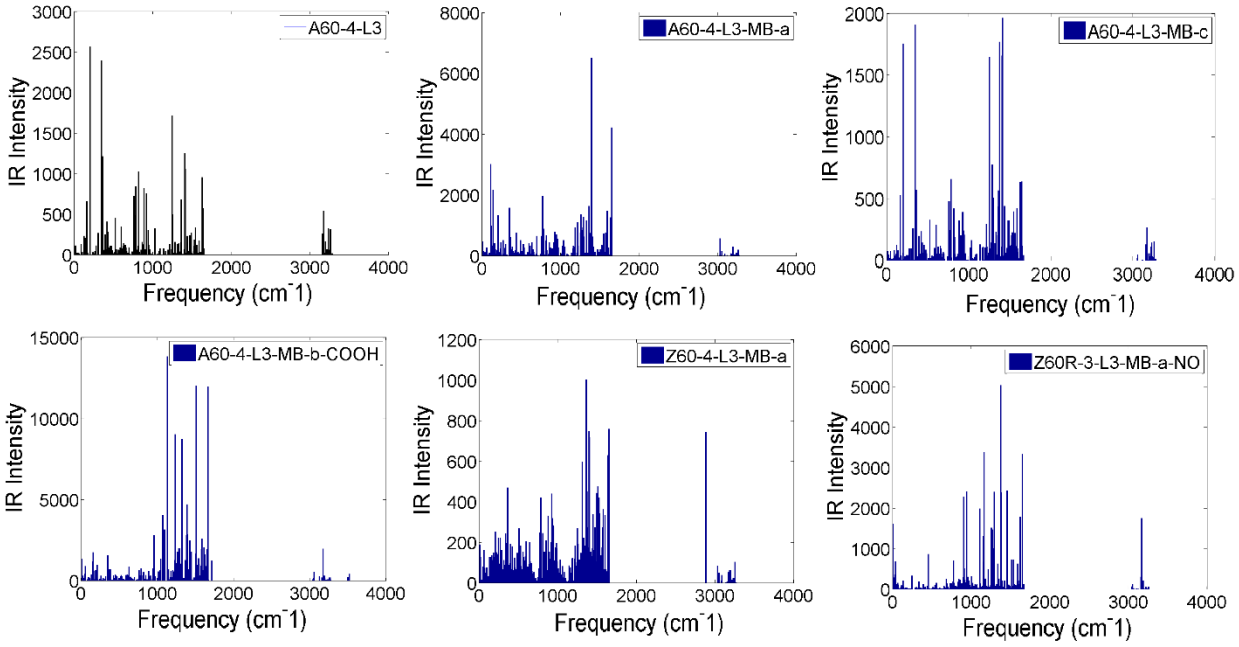

Fig. 4. Inferred spectra of chevron and edge-coved GNR before and after adsorption of MB.

References

[1] Y. Yano, N. Mitoma, H. Ito, and K. Itami, J. Org. Chem. **85**, 4 (2020).

[2] J. Cai, P. Ruffieux, R. Jaafar, M. Bieri, T. Braun, S. Blankenburg, M. Muoth, A. P. Seitsonen, M. Saleh, X. Feng, K. Müllen, and R. Fasel, Nature **466**, 470 (2010).

[3] T. H. Vo, M. Shekhirev, D. A. Kunkel, M. D. Morton, E. Berglund, L. Kong, P. M. Wilson, P. A. Dowben, A. Enders, and A. Sinitskii, Nat. Commun. **5**, 3189 (2014).

[4] A. Narita, X. Feng, Y. Hernandez, S. A. Jensen, M. Bonn, H. Yang, I. A. Verzhbitskiy, C. Casiraghi, M. R. Hansen, A. H. R. Koch, G. Fytas, O. Ivasenko, B. Li, K. S. Mali, T. Balandina, S. Mahesh, S. De Feyter, and K. Müllen, Nat. Chem. **6**, 126 (2014).

[5] P. Ruffieux, S. Wang, B. Yang, C. Sánchez-Sánchez, J. Liu, T. Dienel, L. Talirz, P. Shinde, C. A. Pignedoli, D. Passerone, T. Dumslaff, X. Feng, K. Müllen, and R. Fasel, Nature **531**, 489 (2016).

[6] L. Talirz, P. Ruffieux, and R. Fasel, Adv. Mater. **28**, 6222 (2016).

[7] O. Deniz, C. Sánchez-Sánchez, T. Dumslaff, X. Feng, A. Narita, K. Müllen, N. Kharche, V. Meunier, R. Fasel, and P. Ruffieux, Nano Lett. **17**, 2197 (2017).

[8] V. A. Saroka, K. G. Batrakov, and L. A. Chernozatonskii, Phys. Solid State **56**, 2135 (2014).

[9] V. A. Saroka, K. G. Batrakov, V. A. Demin, and L. A. Chernozatonskii, J. Phys. Condens. Matter **27**, 145305 (2015).

[10] V. A. Saroka and K. G. Batrakov, Russ. Phys. J. **59**, 633 (2016).

[11] V. Saroka, Zigzag-Shaped Graphene Nanoribbons, (2017, August 3) Wolfram Demonstrations Project [Online]. Available: http://demonstrations.wolfram.com/ZigzagShapedGrapheneNanoribbons/.

[12] J. Liu, B.-W. Li, Y.-Z. Tan, A. Giannakopoulos, C. Sanchez-Sanchez, D. Beljonne, P.

Ruffieux, R. Fasel, X. Feng, and K. Müllen, J. Am. Chem. Soc. **137**, 6097 (2015).
[13] D. Beyer, S. Wang, C. A. Pignedoli, J. Melidonie, B. Yuan, C. Li, J. Wilhelm, P. Ruffieux, R. Berger, K. Müllen, R. Fasel, and X. Feng, J. Am. Chem. Soc. **141**, 2843 (2019).
[14] M. Mehdi Pour, A. Lashkov, A. Radocea, X. Liu, T. Sun, A. Lipatov, R. A. Korlacki, M. Shekhirev, N. R. Aluru, J. W. Lyding, V. Sysoev, and A. Sinitskii, Nat. Commun. **8**, 820 (2017).
[15] J. D. Teeter, P. Zahl, M. Mehdi Pour, P. S. Costa, A. Enders, and A. Sinitskii, ChemPhysChem **20**, 2281 (2019).
[16] H. Sakaguchi, S. Song, T. Kojima, and T. Nakae, Nat. Chem. **9**, 57 (2017).
[17] M. Di Giovannantonio, K. Eimre, A. V. Yakutovich, Q. Chen, S. Mishra, J. I. Urgel, C. A. Pignedoli, P. Ruffieux, K. Müllen, A. Narita, and R. Fasel, J. Am. Chem. Soc. **141**, 12346 (2019).
[18] M. Fujita, K. Wakabayashi, K. Nakada, and K. Kusakabe, J. Phys. Soc. Japan **65**, 1920 (1996).
[19] K. Nakada, M. Fujita, G. Dresselhaus, and M. S. Dresselhaus, Phys. Rev. B **54**, 17954 (1996).
[20] D. Pesin and A. H. MacDonald, Nat. Mater. **11**, 409 (2012).
[21] B. Trauzettel, D. V. Bulaev, D. Loss, and G. Burkard, Nat. Phys. **3**, 192 (2007).
[22] R. Hanson, L. P. Kouwenhoven, J. R. Petta, S. Tarucha, and L. M. K. Vandersypen, Rev. Mod. Phys. **79**, 1217 (2007).
[23] M. Slota, A. Keerthi, W. K. Myers, E. Tretyakov, M. Baumgarten, A. Ardavan, H. Sadeghi, C. J. Lambert, A. Narita, K. Müllen, and L. Bogani, Nature **561**, E31 (2018).
[24] J.-W. Rhim, J. Behrends, and J. H. Bardarson, Phys. Rev. B **95**, 035421 (2017).
[25] J.-W. Rhim, J. H. Bardarson, and R.-J. Slager, Phys. Rev. B **97**, 115143 (2018).
[26] V. M. Martinez Alvarez, J. E. Barrios Vargas, M. Berdakin, and L. E. F. Foa Torres, Eur. Phys. J. Spec. Top. **227**, 1295 (2018).
[27] D. J. Thouless, M. Kohmoto, M. P. Nightingale, and M. den Nijs, Phys. Rev. Lett. **49**, 405 (1982).
[28] Y. Hatsugai, Phys. Rev. Lett. **71**, 3697 (1993).
[29] F. D. M. Haldane, Phys. Rev. Lett. **61**, 2015 (1988).
[30] C. L. Kane and E. J. Mele, Phys. Rev. Lett. **95**, 226801 (2005).
[31] D. N. Sheng, Z. Y. Weng, L. Sheng, and F. D. M. Haldane, Phys. Rev. Lett. **97**, 036808 (2006).
[32] C. L. Kane and E. J. Mele, Phys. Rev. Lett. **95**, 146802 (2005).
[33] W. Yao, S. A. Yang, and Q. Niu, Phys. Rev. Lett. **102**, 096801 (2009).
[34] I. Martin, Y. M. Blanter, and A. F. Morpurgo, Phys. Rev. Lett. **100**, 036804 (2008).
[35] W. Li and R. Tao, J. Phys. Soc. Japan **81**, 024704 (2012).
[36] V. M. Martinez Alvarez, J. E. Barrios Vargas, and L. E. F. Foa Torres, Phys. Rev. B **97**, 121401 (2018).
[37] S. Yao and Z. Wang, Phys. Rev. Lett. **121**, 086803 (2018).
[38] F. Song, S. Yao, and Z. Wang, Phys. Rev. Lett. **123**, 246801 (2019).
[39] M. Ezawa, Phys. Rev. B **76**, 245415 (2007).
[40] Z. Z. Zhang, K. Chang, and F. M. Peeters, Phys. Rev. B **77**, 235411 (2008).
[41] M. Zarenia, A. Chaves, G. A. Farias, and F. M. Peeters, Phys. Rev. B **84**, 245403 (2011).
[42] D. R. da Costa, M. Zarenia, A. Chaves, G. A. Farias, and F. M. Peeters, Phys. Rev. B **92**, 115437 (2015).

[43] H. Abdelsalam, M. H. Talaat, I. Lukyanchuk, M. E. Portnoi, and V. A. Saroka, J. Appl. Phys. **120**, 014304 (2016).
[44] K. Kikutake, M. Ezawa, and N. Nagaosa, Phys. Rev. B **88**, 115432 (2013).
[45] H. Abdelsalam, V. A. Saroka, M. Ali, N. H. Teleb, H. Elhaes, and M. A. Ibrahim, Phys. E Low-Dimensional Syst. Nanostructures **108**, 339 (2019).
[46] R. Zhang, X. Y. Zhou, D. Zhang, W. K. Lou, F. Zhai, and K. Chang, 2D Mater. **2**, 045012 (2015).
[47] V. A. Saroka, I. Lukyanchuk, M. E. Portnoi, and H. Abdelsalam, Phys. Rev. B **96**, 085436 (2017).
[48] Z. T. Jiang, S. Li, Z. T. Lv, and X. D. Zhang, AIP Adv. **7**, 045122 (2017).
[49] L. L. Li, D. Moldovan, W. Xu, and F. M. Peeters, Phys. Rev. B **96**, 155425 (2017).
[50] L. L. Li, D. Moldovan, W. Xu, and F. M. Peeters, Nanotechnology **28**, 085702 (2017).
[51] H. Abdelsalam, V. A. Saroka, I. Lukyanchuk, and M. E. Portnoi, J. Appl. Phys. **124**, 124303 (2018).
[52] A. Agarwala and V. B. Shenoy, Phys. Rev. Lett. **118**, 236402 (2017).
[53] T. Cao, F. Zhao, and S. G. Louie, Phys. Rev. Lett. **119**, 076401 (2017).
[54] D. J. Rizzo, G. Veber, T. Cao, C. Bronner, T. Chen, F. Zhao, H. Rodriguez, S. G. Louie, M. F. Crommie, and F. R. Fischer, Nature **560**, 204 (2018).
[55] O. Gröning, S. Wang, X. Yao, C. A. Pignedoli, G. Borin Barin, C. Daniels, A. Cupo, V. Meunier, X. Feng, A. Narita, K. Müllen, P. Ruffieux, and R. Fasel, Nature **560**, 209 (2018).
[56] S. Wang, L. Talirz, C. A. Pignedoli, X. Feng, K. Müllen, R. Fasel, and P. Ruffieux, Nat. Commun. **7**, 11507 (2016).
[57] Y. Lee, F. Zhao, T. Cao, J. Ihm, and S. G. Louie, Nano Lett. **18**, 7247 (2018).
[58] K. I. Ramachandran, G. Deepa, and K. Namboori, *Computational Chemistry and Molecular Modeling*. (Springer, Berlin, 2008).
[59] H. Abdelsalam, V. A. Saroka, and W. O. Younis, Superlattices Microstruct. **129**, 54 (2019).
[60] P. Hohenberg, W. Kohn, Phys. Rev. 136 (1964) 864.
[61] W. Kohn, L.J. Sham, Phys. Rev. 140 (1965) 1133.
[62] M.J. Frisch, G.W. Trucks, H.B. Schlegel, G.E. Scuseria, et al., Gaussian 16, Revision B.01, Gaussian, Inc., Wallingford, CT, 2016.
[63] A.D. Becke, J. Chem. Phys. 98 (1993) 564.
[64] C. Lee, W. Yang, P.G. Parr, Phys. Rev. B 37 (1998) 785.
[65] E. Rudberg, P. Salek, Y. Luo, Nano Lett. 7 (2007) 2211.
[66] H. Abdelsalam, H. Elhaes, M.A. Ibrahim, Chem. Phys. Lett. 696 (2018) 138.
[67] H. Abdelsalam, W. O. Younis, V. A. Saroka, N. H. Teleb, S. Yunoki, Q. Zhang, Phys. Chem. Chem. Phys, 2020, 22, 2566.
[68] P. Shemella, Y. Zhang, M. Mailman, P.M. Ajayan, S.K. Nayak, Appl. Phys. Lett. 91(2007) 042101.
[69] S. Grimme, J. Antony, S. Ehrlich, H. Krieg, J. Chem. Phys. 132, (2010),154104.
[70] F.L. Hirshfeld, Theor. Chim. Acta 44 (1977) 129.
[71] T. D. Veal, I. Mahboob and C. F. McConville, Phys. Rev. Lett., 2004, 92, 136801.
[72] N. Malkova and G. W. Bryant, Phys. Rev. B, 2010, 82, 155314.
[73] N. Malkoval and G. W. Bryant, Physica B 410, 147 (2013).